Simultaneous 8.2 keV phase-contrast imaging and 24.6 keV X-ray diffraction from shock-compressed matter at the LCLS

F. Seiboth, L. B. Fletcher, D. McGonegle, S. Anzellini, L. E. Dresselhaus-Cooper, M. Frost, E. Galtier, S. Goede, M. Harmand, H. J. Lee, A. L. Levitan, K. Miyanishi, B. Nagler, I. Nam, N. Ozaki, M. Rödel, A. Schropp, C. Spindloe, P. Sun, J. S. Wark, J. Hastings, S. H. Glenzer, and E. E. McBride

Citation: Appl. Phys. Lett. **112**, 221907 (2018); doi: 10.1063/1.5031907

View online: https://doi.org/10.1063/1.5031907

View Table of Contents: http://aip.scitation.org/toc/apl/112/22

Published by the American Institute of Physics

Simultaneous 8.2 keV phase-contrast imaging and 24.6 keV X-ray diffraction from shock-compressed matter at the LCLS

F. Seiboth,[1,2] L. B. Fletcher,[1] D. McGonegle,[3] S. Anzellini,[4] L. E. Dresselhaus-Cooper,[5] M. Frost,[1] E. Galtier,[1] S. Goede,[6] M. Harmand,[7] H. J. Lee,[1] A. L. Levitan,[1] K. Miyanishi,[8] B. Nagler,[1] I. Nam,[1] N. Ozaki,[8,9] M. Rödel,[10,11] A. Schropp,[2] C. Spindloe,[12] P. Sun,[1] J. S. Wark,[3] J. Hastings,[1] S. H. Glenzer,[1] and E. E. McBride[1,6,a)]

[1]*SLAC National Accelerator Laboratory, 2575 Sand Hill Road, Menlo Park, California 94025, USA*
[2]*Deutsches Elektronen-Synchrotron DESY, Notkestrasse 85, D-22607 Hamburg, Germany*
[3]*Department of Physics, Clarendon Laboratory, University of Oxford, Parks Road, Oxford OX1 3PU, United Kingdom*
[4]*Diamond Light Source Ltd., Harwell Science and Innovation Campus, OX11 0DE Didcot, United Kingdom*
[5]*Department of Chemistry, Massachusetts Institute of Technology, Cambridge, Massachusetts 02139, USA*
[6]*European XFEL GmbH, Holzkoppel 4, D-22869 Schenefeld, Germany*
[7]*Sorbonne Université, Muséum National d'Histoire Naturelle, UMR CNRS 7590, IRD, Institut de Minéralogie, de Physique des Matériaux et de Cosmochimie, IMPMC, 4 Place Jussieu, 75005, Paris, France*
[8]*Institute for Laser Engineering, Osaka University, 2-6 Yamadaoka, Suita, Osaka, 565-0871 Japan*
[9]*Photon Pioneers Center, Osaka University, Suita, Osaka 565-0871, Japan*
[10]*Helmholtz-Zentrum Dresden-Rossendorf, P.O. Box 510119, D-01314 Dresden, Germany*
[11]*Technische Universität Dresden, D-01069 Dresden, Germany*
[12]*Central Laser Facility, STFC, Rutherford Appleton Laboratory, Harwell Oxford, Didcot OX11 0QX, United Kingdom*

(Received 2 April 2018; accepted 28 April 2018; published online 1 June 2018)

In this work, we demonstrate simultaneous phase-contrast imaging (PCI) and X-ray diffraction from shock compressed matter at the Matter in Extreme Conditions endstation, at the Linac Coherent Light Source (LCLS). We utilize the chromaticity from compound refractive X-ray lenses to focus the 24.6 keV 3rd order undulator harmonic of the LCLS to a spot size of 5 μm on target to perform X-ray diffraction. Simultaneous PCI from the 8.2 keV fundamental X-ray beam is used to visualize and measure the transient properties of the shock wave over a 500 μm field of view. Furthermore, we demonstrate the ability to extend the reciprocal space measurements by 5 Å^{-1}, relative to the fundamental X-ray energy, by utilizing X-ray diffraction from the 3rd harmonic of the LCLS.
https://doi.org/10.1063/1.5031907

Knowledge of the behavior of matter at extreme pressures and temperatures is necessary for understanding materials at the core of giant planets, in impact events, and in nuclear fusion processes.[1–3] One avenue to create such matter is through laser-driven shock compression, whereby Mbar pressures and eV temperatures may be generated over nanosecond timescales. The ∼100 fs hard X-ray pulses produced by the Linac Coherent Light Source (LCLS), are essential for investigating the structure and behavior of matter at extreme conditions. In such dynamic compression experiments, *in-situ* X-ray diffraction has been proven to be a key diagnostic, and numerous studies to date have combined this technique with high power nanosecond laser drivers at the Matter in Extreme Conditions (MEC) endstation at the LCLS.[1,2,4–11]

In many shock wave experiments, the material conditions inferred are diagnosed using optical velocimetry (VISAR),[12] an interferometric technique whereby the velocity of a reflecting rear surface is measured as a shock wave exits it. However, this technique does not provide direct structural information, and provides limited insight into how the complex waves behave inside the sample.

Hard X-ray free-electron lasers, like the LCLS, provide an avenue to image shock waves inside optically opaque samples. Schropp *et al.*, have demonstrated the ability to measure the properties of a shock wave as it progresses through a sample using a phase-contrast imaging (PCI) technique.[13] Since shock waves typically travel through samples at speeds of a few μm/ns, the 100 fs duration of the X-ray pulses available at the LCLS allows one to take a snapshot of the shock wave as it traverses the sample. However, in such a configuration the large illumination spot necessary for imaging will diffract from several hundred microns of the sample, scattering from both the static uncompressed sample and the high-pressure, high-temperature states generated by the shock wave, within a typically far smaller optical focal spot. Therefore, it becomes increasingly difficult to discern the nature of the high pressure phase as diffraction patterns can be dominated by scattering from the uncompressed sample. Furthermore, as one is illuminating the entire shock wave, it is challenging to resolve the onset of phase transitions.

In this letter, we present simultaneous phase-contrast imaging of a shock wave propagating through optically-opaque laser shock-compressed germanium (Ge), combined with X-ray diffraction from a specific region of the sample. Ge was chosen as the crystal of study as it exhibits a complex multi-wave response following dynamic loading, which would display clear signatures in both imaging and diffraction.[14–16] We achieve the simultaneous imaging and diffraction by using

a)Electronic mail: emcbride@slac.stanford.edu

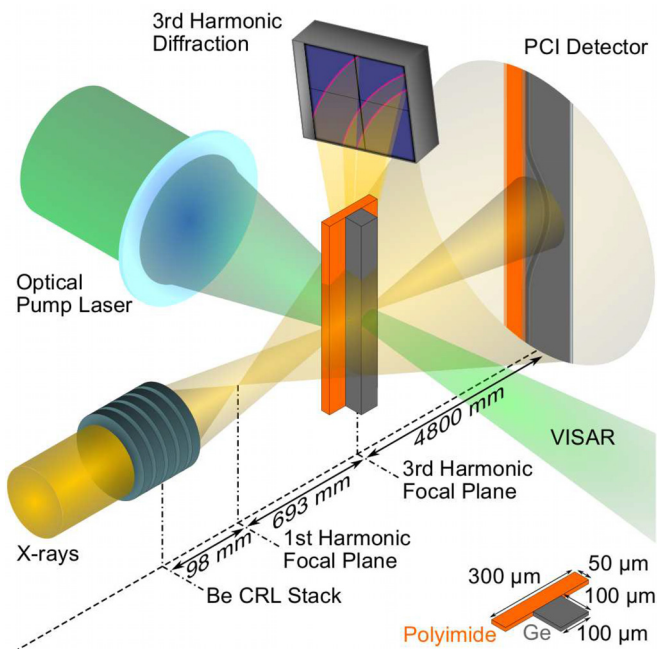

FIG. 1. Experimental setup for simultaneous phase-contrast imaging and X-ray diffraction from shock-compressed matter. The X-ray beam is perpendicular to the optical pump laser used to generate the shock wave in the multi-layer target near the focal place of the 3rd harmonic beam.

the fundamental X-ray beam at 8.2 keV to perform the imaging, and the 24.6 keV X-rays in the 3rd harmonic of the LCLS to perform X-ray diffraction measurements. We take advantage of the wavelength dependence of the X-ray focusing optics to create a micron sized X-ray spot with the 24.6 keV X-rays, which is centered on the large illuminating field of the fundamental X-rays at 8.2 keV. This is an important demonstration of using high X-ray energy to probe dense, high-Z matter.

Experiments were conducted at the MEC endstation[17] at the LCLS using the PCI instrument.[18] Single crystal samples of Ge, with 50 μm polyimide ablators, were shock compressed via irradiation with the nanosecond pulsed Nd:glass laser system. A schematic of the setup used may be seen in Fig. 1. The laser light was frequency-doubled to 527 nm, and a 50 ns temporally square pulse was combined with phase plate optics to produce a 250 μm spot on the ablator surface.[19] This setup provided laser intensities in the range 6.1×10^{11} W/cm^2–1.4×10^{12} W/cm^2 on target. In this work, a transverse geometry was employed, where the X-ray probe beam was incident perpendicular to the shock propagation direction. The X-ray pulse length, generated by self-amplified spontaneous emission (SASE) from the LCLS, was approximately 80 fs, and the jitter between the optical drive laser and the X-ray beam was ± 10 ps.[17]

The target configuration may be seen in Fig. 1. Discs of single crystal Ge, oriented in the [110] direction (Semiconductor Wafer, Inc.), were polished to a thickness of 100 μm, and diced to dimensions of 100 μm (X-ray direction) $\times$ 100 μm (shock direction) $\times$ 2 mm. Bonded to the drive surface (the surface upon which the shock laser was incident), was 50 μm of polyimide, with a 100 nm flash coating of aluminum to prevent the penetration of drive light at early time, and hence prevent tamped ablation. The targets

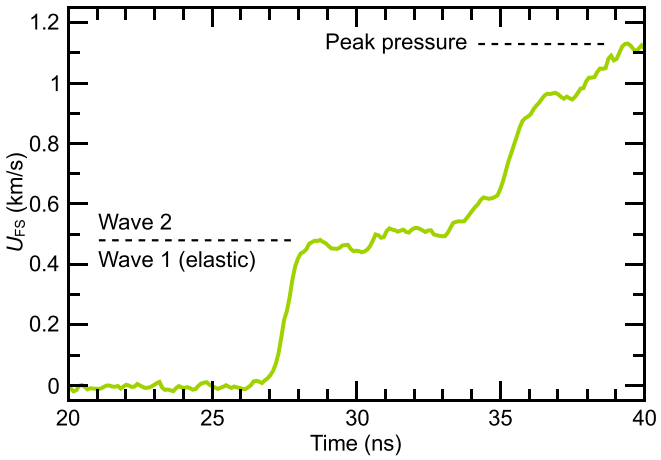

FIG. 2. Velocimetry data (VISAR) lineout showing free-surface velocity U_{FS}. The dashed lines indicate the onset of the 2nd wave, and the peak pressure reached.

were 100 μm in the X-ray direction and the polyimide ablator was 300 μm wide, extended to shield the laser light from hitting the side of the target.

VISAR measurements were recorded on every shot to determine the wave profile as a function of laser intensity. Furthermore, this diagnostic allowed the sample pressure to be inferred using the Rankine-Hugoniot relations. Figure 2 shows a 1D velocity-time trace of a typical shock wave in Ge. In this work, $t = 0$ ns is defined as when the rising edge of the laser drive pulse is incident on the ablator surface. We observe, consistent with previous studies, a strong elastic response, beginning at 27 ns, reaching a peak velocity of $\sim$0.5 km/s, corresponding to a Hugoniot Elastic Limit (HEL) of 5 GPa.[14–16] Following the strong elastic wave, a second wave emerges, and the material is compressed up to a peak-pressure state of 12 GPa.

A stack of beryllium compound refractive lenses (Be CRLs)[20] were used, consisting of 57 individual bi-concave lenses, each with a radius of curvature of 50 μm and a geometric aperture of 300 μm. The chromaticity of the optics allows one to focus higher energy 24.6 keV (3rd harmonic beam) photons directly on target, while simultaneously imaging the sample via magnified PCI by focussing the lower energy 8.2 keV (fundamental beam) photons further upstream, as depicted in Fig. 1.

We used the fundamental undulator harmonic at 8.2 keV for PCI, at which the Be CRL has a numerical aperture (NA) of 0.93×10^{-3} and a focal length of $f_1 = 98$ mm. Diffraction data were collected with the 3rd undulator harmonic at 24.6 keV. Here, the Be CRL has an NA of 0.17×10^{-3} and a focal length of $f_3 = 791$ mm. The position of the 3rd harmonic focal plane was determined by moving a copper grid (1000 mesh, Gilder Grids) along the optical axis, through the focal plane in 10 mm steps, performing a linear regression on the field of view. To tailor the beamsize on target for X-ray diffraction measurements with the 3rd harmonic to approximately 5 μm in diameter the sample was moved downstream from the focal plane by $z_\Delta = 20.5$ mm. The distance from the fundamental focal plane to the target is geometrically fixed at $z_s = f_3 - f_1 + z_\Delta = 713.5$ mm, resulting in a spot size on target of 2.2 mm for the fundamental. Taking into account

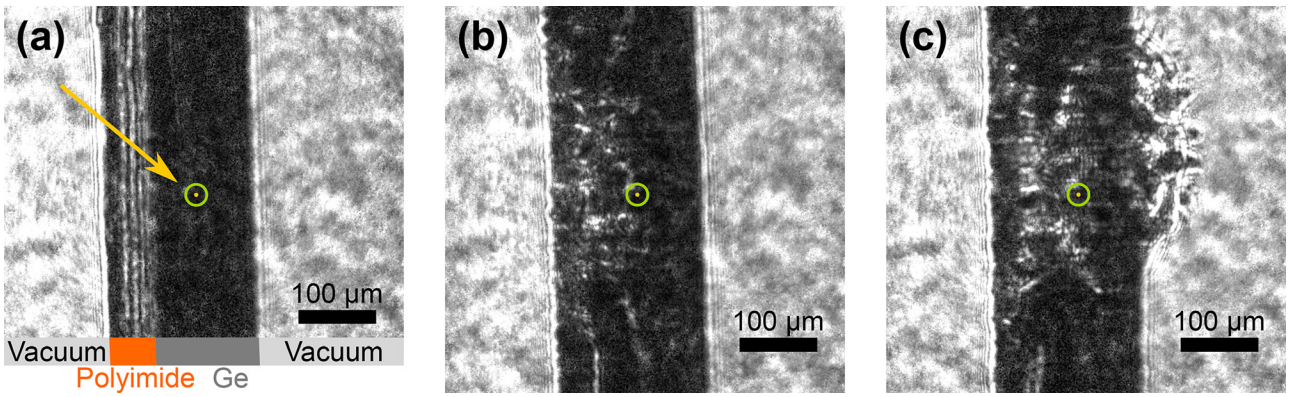

FIG. 3. Phase-contrast images from shock-compressed single crystal Ge. (a) Phase-contrast image before the shock. The yellow dot at the centre of the green circle, marked by the arrow, represents the position and size of the 3rd harmonic on target. One may see the polyimide ablator and Ge sample layers, labeled. (b) Phase-contrast image at $t = 30$ ns after shock initiation at the ablator surface, and (c) phase-contrast image at $t = 40$ ns after shock initiation at the ablator surface.

both the beamline and CRL stack transmission, the X-ray intensity for a single pulse on target was determined to be $\sim 6.7 \times 10^9$ W/cm^2 at 8.2 keV and $\sim 1.7 \times 10^1$ W/cm^2 at 24.6 keV. The PCI detector was placed at a distance $z_d = 4800$ mm downstream of the 3rd harmonic focal plane (cf. Fig. 1) resulting in a magnification of $M = (z_s + z_d)/z_s = 7.7$.

For imaging we used a high-resolution YAG:Ce scintillator based X-ray camera with an effective pixel size of 2.25 μm. In the given geometry this leads to an effective pixel size of 292 nm in the phase-contrast images. The YAG:Ce scintillator had a thickness of 50 μm and absorbs 80% of the fundamental, and 33% of the 3rd harmonic. In order to pinpoint the position of the 3rd harmonic in the field of view of the magnified image from the fundamental, we filtered the fundamental by Si attenuators, effectively only imaging the 3rd harmonic.

X-ray diffraction patterns were collected in transmission through the sample in a Debye-Scherrer geometry on Cornell Stanford Pixellated Area Detectors (CSPADs) at a sample-detector distance of 300 mm. Three CSPADs were used to cover a 2θ range of between 4.5° to 26.5°, 4.5° to 23.1°, and 27.0° to 37.4°, corresponding to a Q-range of between 1 Å^{-1} and 8 Å^{-1}. The equivalent Q-range that would be probed by the 8.2 keV X-rays on the same detectors would be 0.33 Å^{-1}–2.67 Å^{-1}. To ensure that the X-ray diffraction patterns measured were due to scattering from the 3rd harmonic at 24.6 keV, and not due to scattering from the fundamental 8.2 keV beam, 500 μm of aluminum foil was used on the detector active area as a filter. The transmission of 8.2 keV X-rays through 500 μm of Al is 0.25%, whereas for 24.6 keV the transmission is 79.1%.

Figure 3 shows an example of PCI data. Figure 3(a) shows a reference measurement taken from an uncompressed sample. PCI of shock-compressed Ge is shown in Figs. 3(b) and 3(c), where the X-rays probed at 30 ns and 40 ns, respectively. The break out time of the elastic wave, $t = 27$ ns, is determined from the velocimetry data in Fig. 2. In Fig. 3(b), the shock wave has traversed the sample. Although the X-rays were timed at 30 ns, 3 ns after the breakout time as determined by the VISAR there is no evidence of spall in the imaging data. In Fig. 3(c), the X-rays probed at 40 ns. The elastic shock wave break out at the Ge/vacuum interface on the right of Fig. 3(c), and was followed by the 2nd wave. These waves were then reflected back into the Ge sample, interacting with the shock wave, creating an off-Hugoniot state. It is worth noting the ns-drive laser ($t = 50$ ns) is still driving a forward-moving shock into the sample while the X-rays probe the sample. Therefore, PCI can be used to observe such complex wave interactions that result from these reflecting waves within the target.

The 5 μm spot size of the 24.6 keV 3rd harmonic is centered on the spot illuminated by the fundamental beam, thereby allowing accurate spatial probing of the material conditions relative to the position of the shock wave that is simultaneously imaged with PCI. The position and size of the 24.6 keV X-ray beam used for diffraction is shown by the small yellow spot, concentric to the green circle in Fig. 3. Figure 4 shows 1D integrated X-ray diffraction patterns

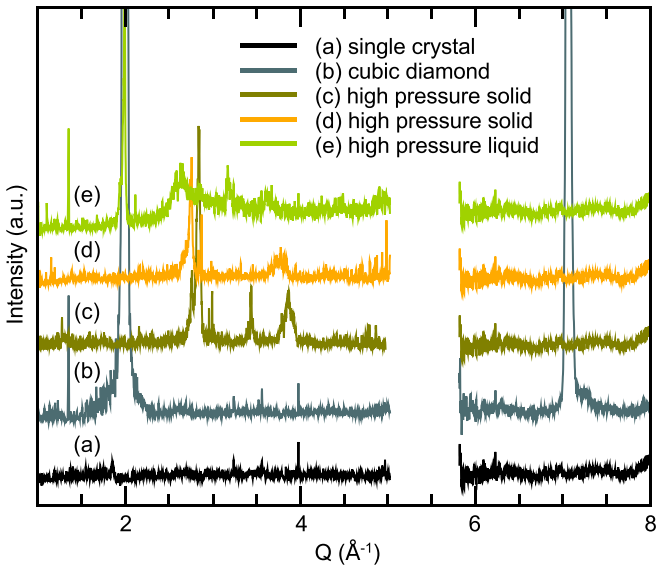

FIG. 4. X-ray diffraction using the 3rd harmonic demonstrating scattering out to a Q range of 8 Å^{-1}, showing diffraction from (a) the uncompressed single crystal, (b) the compressed cubic diamond phase, (c) the high pressure solid phase corresponding to Fig. 3(b) at $t = 30$ ns, (d) the high pressure solid phase corresponding to Fig. 3(c) at $t = 40$ ns, and (e) a high pressure liquid phase. Diffraction patterns are ordered from (a) to (e) in terms of increasing laser intensity. Missing data points arise from angular gaps due to the positioning of the CSPAD detectors.

using the 24.6 keV X-rays. The Ge is initially a single crystal, the Bragg condition is not satisfied on the limited θ–ϕ space covered by the CSPAD, resulting in an integrated 1D pattern with no measurable X-ray signal (black line) Fig. 4(a).

X-ray diffraction patterns corresponding to the PCI data in Figs. 3(b) and 3(c) are shown in Figs. 4(c) and 4(d), respectively. As a consequence of the shock wave, the single crystal breaks up into small nanometer-scale grains, resulting in powder-like rings on the CSPAD detector. The evidence of a high pressure solid structure may be seen by the appearance of sharp peaks at 2.7 Å^{-1} and 3.8 Å^{-1}. The peak in Fig. 4(c) at 3.4 Å^{-1} is due to scattering from the compressed ambient pressure phase which has been rotated into the X-ray beam due to the shock wave.

Although we have focussed on demonstrating simultaneous PCI and X-ray diffraction, and have shown how useful this technique can be when investigating shock-compressed materials, in particular those which exhibit complex multi-wave features, or targets undergoing release, there are other advantages to using the much higher X-ray energies available in the 3rd harmonic. Figures 4(b) and 4(e) show additional examples of the X-ray diffraction possible at 24.6 keV. A distinct advantage of using such a high X-ray energy is that for the same 2θ range, one may access a significantly larger Q range. Here, we can measure an X-ray signal to a Q of 8 Å^{-1} for a scattering angle of 47°. Using the highest stable energy of the fundamental beam—of about 11 keV—one may only reach a Q of 3.6 Å^{-1} over this same angular range. Taking advantage of a higher X-ray energy allows for direct X-ray probing of atomic scale structures over a larger range of reciprocal space. Such information may be necessary when investigating the nature of phase transitions under dynamic processes.

Figure 4(b) shows diffraction from a compressed single crystal of the cubic diamond phase of Ge, which has been rotated into the X-ray beam, satisfying the Bragg condition. One may see the (111) reflection at 2.00 Å^{-1}, corresponding to a lattice parameter of the cubic diamond structure of $a = 5.44$ Å, and a V/V_0 of 0.89. The peak at 7.06 Å^{-1} corresponds to the (531) reflection of the uncompressed cubic diamond structure.

At the highest laser intensities and hence highest pressures reached, the sample was observed to melt completely, as shown by the disappearance of Bragg scattering and appearance of the broad diffuse feature at 2.7 Å^{-1} [Fig. 4(e)], and the possibility of a weaker diffuse feature at 5 Å^{-1} indicating the second coordination shell (subject to further analysis). This is consistent with previous high pressure X-ray diffraction studies of liquid Ge.[21]

In conclusion, we have implemented an experimental platform to perform simultaneous phase-contrast imaging with microfocussed X-ray diffraction using both the fundamental and 3rd harmonic of the LCLS. We have directly observed complex wave interactions within the sample that arise during both shock and release, and have isolated such structures in the same shot with a microfocussed 24.6 keV beam for X-ray diffraction. Furthermore, we have demonstrated proof-of-principle diffraction patterns, including liquid scattering, using the 3rd harmonic of the LCLS, allowing one to access a significantly higher Q range. Such structural information is vital for understanding the properties of matter at extreme pressures and temperatures.

F. Seiboth and E. E. McBride acknowledge funding from the Volkswagen Foundation. D. McGonegle was supported by LLNS under Contract No. B595954. J. S. Wark is grateful for support from EPSRC under Grant No. EP/J017256/1. This work was supported by the French Agence Nationale de la Recherche (ANR) with the ANR IRONFEL 12-PDOC-0011. This project has received funding from the European Research Council (ERC) under the European Union's Horizon 2020 research and innovation program (ERC PLANETDIVE, grant agreement No. 670787). Use of the Linac Coherent Light Source (LCLS), SLAC National Accelerator Laboratory, is supported by the U.S. Department of Energy, Office of Science, Office of Basic Energy Sciences under Contract No. DE-AC02-76SF00515. The MEC instrument is supported by the U.S. Department of Energy, Office of Science, Office of Fusion Energy Sciences under Contract No. SF00515. The PCI setup was funded in parts by the German Ministry of Education and Research (BMBF) under Grant No. 05K13OD2. SLAC High Energy Density Science Division acknowledges support from FES No. FWP100182.

[1]D. Kraus, A. Ravasio, M. Gauthier, D. Gericke, J. Vorberger, S. Frydrych, J. Helfrich, L. Fletcher, G. Schaumann, B. Nagler *et al.*, Nat. Commun. **7**, 10970 (2016).
[2]A. E. Gleason, C. A. Bolme, H. J. Lee, B. Nagler, E. Galtier, D. Milathianaki, J. Hawreliak, R. G. Kraus, J. H. Eggert, D. E. Fratanduono *et al.*, Nat. Commun. **6**, 8191 (2015).
[3]S. Glenzer, B. MacGowan, P. Michel, N. Meezan, L. Suter, S. Dixit, J. Kline, G. Kyrala, D. Bradley, D. Callahan *et al.*, Science **327**, 1228 (2010).
[4]M. Gorman, R. Briggs, E. McBride, A. Higginbotham, B. Arnold, J. Eggert, D. Fratanduono, E. Galtier, A. Lazicki, H. Lee *et al.*, Phys. Rev. Lett. **115**, 095701 (2015).
[5]A. Gleason, C. Bolme, E. Galtier, H. Lee, E. Granados, D. Dolan, C. Seagle, T. Ao, S. Ali, A. Lazicki *et al.*, Phys. Rev. Lett. **119**, 025701 (2017).
[6]D. Kraus, J. Vorberger, A. Pak, N. Hartley, L. Fletcher, S. Frydrych, E. Galtier, E. Gamboa, D. Gericke, S. Glenzer *et al.*, Nat. Astron. **1**, 606 (2017).
[7]C. Wehrenberg, D. McGonegle, C. Bolme, A. Higginbotham, A. Lazicki, H. Lee, B. Nagler, H.-S. Park, B. Remington, R. Rudd *et al.*, Nature **550**, 496 (2017).
[8]A. Gleason, C. Bolme, H. Lee, B. Nagler, E. Galtier, R. Kraus, R. Sandberg, W. Yang, F. Langenhorst, and W. Mao, Nat. Commun. **8**, 1481 (2017).
[9]R. Briggs, M. Gorman, A. Coleman, R. McWilliams, E. McBride, D. McGonegle, J. Wark, L. Peacock, S. Rothman, S. Macleod *et al.*, Phys. Rev. Lett. **118**, 025501 (2017).
[10]L. Fletcher, H. Lee, T. Döppner, E. Galtier, B. Nagler, P. Heimann, C. Fortmann, S. LePape, T. Ma, M. Millot *et al.*, Nat. Photonics **9**, 274 (2015).
[11]A. Schropp, J. Patommel, F. Seiboth, B. Arnold, E. C. Galtier, H. J. Lee, B. Nagler, J. B. Hastings, and C. G. Schroer, in *SPIE Optical Engineering+Applications* (International Society for Optics and Photonics, 2012), pp. 85040F–85040F.
[12]L. Barker and R. Hollenbach, J. Appl. Phys. **43**, 4669 (1972).
[13]A. Schropp, R. Hoppe, V. Meier, J. Patommel, F. Seiboth, Y. Ping, D. G. Hicks, M. A. Beckwith, G. W. Collins, A. Higginbotham *et al.*, Sci. Rep. **5**, 11089 (2015).
[14]W. Gust and E. Royce, J. Appl. Phys. **43**, 4437 (1972).
[15]R. A. Graham, O. E. Jones, and J. R. Holland, J. Phys. Chem. Solids **27**, 1519 (1966).
[16]S. J. Ali, C. A. Bolme, G. W. Collins, and R. Jeanloz, Rev. Sci. Instrum. **86**, 043112 (2015).

[17]B. Nagler, B. Arnold, G. Bouchard, R. F. Boyce, R. M. Boyce, A. Callen, M. Campell, R. Curiel, E. Galtier, J. Garofoli *et al.*, J. Synchrotron Radiat. **22**, 520 (2015).
[18]B. Nagler, A. Schropp, E. C. Galtier, B. Arnold, S. B. Brown, A. Fry, A. Gleason, E. Granados, A. Hashim, J. B. Hastings, D. Samberg, F. Seiboth, F. Tavella, Z. Xing, H. J. Lee, and C. G. Schroer, Rev. Sci. Instrum. **87**, 103701 (2016).
[19]S. Dixit, K. Nugent, J. Lawson, K. Manes, and H. Powell, Opt. Lett. **19**, 417 (1994).
[20]B. Lengeler, C. Schroer, J. Tummler, B. Benner, M. Richwin, A. Snigirev, I. Snigireva, and M. Drakopoulos, J. Synchrotron Radiat. **6**, 1153 (1999).
[21]J. Kōga, H. Okumura, K. Nishio, T. Yamaguchi, and F. Yonezawa, Phys. Rev. B **66**, 064211 (2002).